PERGAMON

International Journal of Multiphase Flow 28 (2002) 1351–1368

International Journal of Multiphase Flow

www.elsevier.com/locate/ijmulflow

Local flow characteristics of subcooled boiling flow of water in a vertical concentric annulus

T.H. Lee [a,*], G.C. Park [b], D.J. Lee [a]

[a] *Power Reactor Technology Development Division, Korea Atomic Energy Research Institute, P.O. Box 105, Yusung, Taejon 305-600, South Korea*

[b] *Department of Nuclear Engineering, Seoul National University, San 56-1, Shinlim-dong, Gwanak-gu, Seoul, 151-742, South Korea*

Received 9 January 2002; received in revised form 25 March 2002

Abstract

The radial profiles of local void fraction and velocities of both phases were measured in subcooled boiling flow of water in a vertical concentric annulus with a heated inner tube. A two-conductivity probe technique was used for the measurements of local void fraction and vapor velocity and a Pitot tube method was applied to measure the local liquid velocity. Measurements were performed under various conditions of mass flux, heat flux, and inlet subcooling. Based on the measurements, the influence of such flow conditions on the distributions of local flow parameters was investigated. Also, some measurements have been compared to the predictions by the three-dimensional two-fluid model of subcooled boiling flow in the computer code CFX-4.2.

Keywords: Void fraction; Vapor velocity; Liquid velocity; Subcooled boiling; Two-conductivity probe; Pitot tube; CFX-4.2

1. Introduction

Fundamental experiments for obtaining an accurate knowledge of distributions of the local two-phase flow parameters are crucial to the eventual understanding and modeling of interfacial transfer terms which are required in a mechanistic multidimensional analysis of a two-phase flow field. Thus, for the purpose of providing basic information on the local flow field and interfacial

* Corresponding author: Tel.: +82-42-868-8975; fax: +82-42-868-8990.
E-mail address: thlee@kaeri.re.kr (T.H. Lee).

0301-9322/02/$ - see front matter © 2002 Published by Elsevier Science Ltd.
PII: S0301-9322(02)00026-5

transfer mechanism, extensive experimental studies for local measurements in two-phase flow have been carried out. However, most of the studies have been restricted to the adiabatic two-phase flow (Serizawa et al., 1975; Herringe and Davis, 1976; Welle, 1985; Kataoka et al., 1986; Liu, 1989; Kocamustafaogullari and Wang, 1991; Revankar and Ishii, 1992; Velidandla et al., 1996).

In spite of a lot of work in adiabatic gas–liquid flow, the local measurements in subcooled boiling are very limited so far. Moreover, much of the previous works have dealt understandably with measurements of gross effects rather than local effects. The earliest experiment on local effects in the subcooled boiling flow was by Jiji and Clark (1964). Miniature thermocouples were used to measure the temperature distributions in a boiling layer of water. However, their measurements did not provide the detailed temperature characteristics since the time constant of the thermocouple was too high to detect the temperature fluctuation accurately. Delhaye et al. (1973) developed a fast microthermocouple that could enable the detection of vapor or liquid phase and the temperature measurement of each phase, and performed measurements of local void fraction and temperatures of liquid and vapor in steam–water flow. The local void fraction was estimated from the probability density function of the temperature signal. Sekoguchi et al. (1981) used the electric resistivity probe technique to measure both radial and axial distributions of local void fraction in subcooled and low quality boiling flow of water through cylindrical tubes. Hino and Ueda (1985) measured the spatial distributions of local mixture average temperature and its fluctuation using chromel-constantan microthermocouples for R-113 subcooled boiling flow in a vertical annular channel. The probability density functions of the local mixture temperature were derived. Also, the power spectra of mixture temperature fluctuations, the distributions of bubble frequency and resident time intervals of vapor and liquid were reported. Hasan et al. (1991) measured the radial profiles of mixture mean liquid temperature and void fraction in subcooled boiling of R-113 through a vertical annulus. The fluid temperature was measured by a chromel-constantan microthermocouple and the void fraction by a cylindrical hot-film sensor. However, the vapor temperature could not be measured due to the relatively slow response of microthermocouple. Recently, Roy et al. (1997) measured the void fraction and the velocity field in subcooled boiling flow of R-113 through a vertical annulus. The void faction was measured by optical fiber probe. The vapor velocity was measured by two-component LDV and optical fiber probe. Also, the liquid velocity was measured by two-component LDV. The near-wall liquid velocity field was found to be quite different from that in single-phase liquid flow at a similar Reynolds number. Besides the works stated above, some additional works on local measurements have been reported in the literature. However, more comprehensive information is needed for understanding of detailed physics of subcooled boiling phenomenon. Thus, appropriate fundamental experiments for obtaining the information on the local flow structure in subcooled boiling is still required for deeper insights into the physics of the boiling phenomenon.

Multidimensional analyses of subcooled boiling flow are also very few. Recently, Roy et al. (1997) analyzed the subcooled flow boiling of R-113 in a vertical annulus using the computer code, ASTRID (Briere et al., 1995) and compared the results with their measurement data. The comparison of the results with the measured void fraction, vapor velocity, liquid velocity and liquid temperature showed reasonable agreement. However, the difference between prediction and measurement, especially near inner heated wall, pointed out the need for further modeling works.

In this study, the radial profiles of local void fraction, vapor velocity and liquid velocity were measured in the subcooled boiling flow of water in a vertical concentric annulus having a heated inner tube. Using a two-conductivity probe technique, the local values of void fraction and vapor velocity were measured. Also, Pitot tube method was applied to measure the local liquid velocity. Measurements were radially made at one axial plane of the channel for different levels of mass flux, heat flux, and inlet subcooling. Based on the measurements, the local flow structure of subcooled boiling was investigated. Also, some measurements were compared with the predictions of the multidimensional two-fluid model of subcooled boiling in a computer code CFX-4.2 to assess the capability of the various implemented boiling two-phase flow models.

2. Experiments

2.1. Test loop

A schematic of the test loop is shown in Fig. 1. The test loop consists mainly of the test channel, water storage tank, circulating pump, preheater and water purification unit. Distilled and de-gassed water from the storage tank is pumped and flows through a turbine flowmeter and a preheater to the bottom of the test channel. The test channel contains a heated section where the subcooled boiling occurs. The two-phase mixture at the channel outlet flows back to the storage tank where vapor bubbles are condensed by cooling coils.

The test channel is a vertical concentric annulus, 2376 mm long with a heated inner tube. The inner tube of 19 mm in outer diameter is composed of a heated section and two unheated sections. The heated section is a 1670 mm long Inconel 625 tube with 1.5 mm wall thickness, and is filled

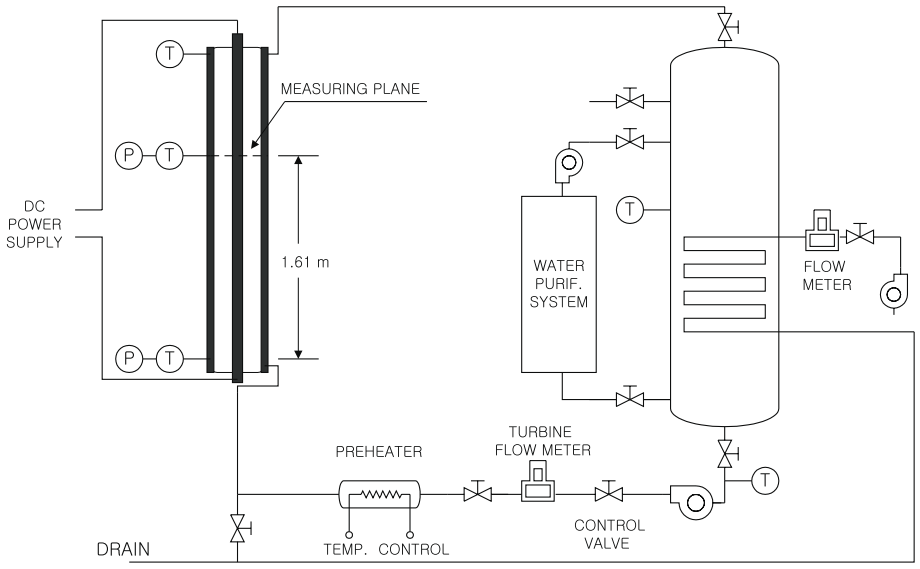

Fig. 1. Schematic of test loop.

with magnesium oxide powder insulation. This heated section is preceded and followed by 280 mm long and 610 mm long, thick-walled copper tubes, respectively. The inner tube is connected to a 54 kW DC power supply and uniformly generates the heat in the heated middle section. The outer tube is comprised of two stainless steel tubes with 37.5 mm inner diameter, which are connected by a transparent glass tube so that visual observation or photographing is possible. The transparent glass tube is 50 mm long, and is located below the measuring plane. The measuring plane is located at 1610 mm downstream of the beginning of the heated section. Also, the test channel is thermally insulated by glass wool, except for the glass tube. Traversing units, composed of ball slide units and microverniers with 0.01 mm spatial resolution, are used to move the local probes in the direction perpendicular to the axis of the test channel.

To prevent the heated surface from contaminating by ions of potentially insoluble component from water, a small amount of water ($\sim$4 lpm) is recirculated through the water purification unit during experiments, which is composed of heat exchanger, demineralizer and filters. The specific resistivity of recirculating water is maintained to 2 MΩ/cm.

2.2. Measurements

The test channel inlet and exit temperatures as well as the liquid temperature outside the bubble boundary layer at the measuring plane were measured using the calibrated platinum resistance temperature detectors. The uncertainty of temperature measurement was estimated to be $\pm$0.2 °C. The uncertainties in the measurements of the present experiments were estimated by random error and bias error with 95% confidence. The absolute pressures were measured at inlet and measuring plane with the estimated uncertainties of $\pm$0.001 and $\pm$0.0005 MPa, respectively. The mass flux was determined with the inlet volumetric flow rate measured by turbine flowmeter, water density and flow area. The uncertainty was estimated to be $\pm$1.9% of the rated mass flux. The test channel inlet temperature was controlled by a preheater which has a maximum capacity of 50 kW. The inlet subcooling was calculated from the measured temperature and absolute pressure at inlet and the uncertainty was estimated to be $\pm$0.3 °C. Heat flux was calculated from the measured voltage drop across the heated tube, the current through it and the heated surface area. It was controlled by a DC power supply and the uncertainty was estimated to be $\pm$1.7% of the rated heat flux. Heat balance in the single-phase liquid flow was also checked across the test channel to examine the accuracy of the heat flux calculation. The heat flux, which was calculated from the liquid flow rate and the temperature increase between the test channel inlet and outlet, was estimated to be less than 1.7% of the value calculated from the measured current and voltage drop, which was due to the heat loss around the test section.

2.2.1. Two-conductivity probe method

The local vapor phase parameters such as void fraction and vapor velocity were measured by a two-conductivity probe method. The conductivity probe method is based on the use of the difference of electrical resistance between vapor and liquid phases. The concept of the method was first proposed by Neal and Bankoff (1963). After that Serizawa et al. (1975), Herringe and Davis (1976), Welle (1985) and Liu (1989) extended it to a two-conductivity probe method for measuring local gas-phase parameters such as local void fraction, bubble velocity, bubble frequency and bubble diameter in vertical air–water bubbly flow. Also, Kocamustafaogullari and Wang (1991)

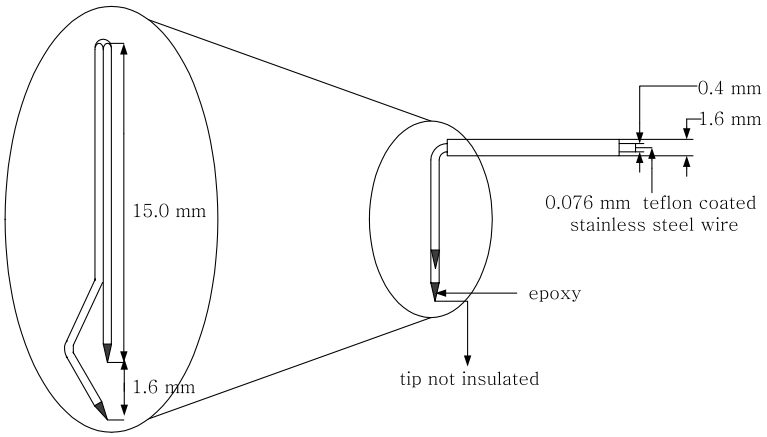

Fig. 2. Schematic of two-conductivity probe.

applied the method to the measurements of local interfacial parameters in horizontal air–water bubbly flow where local void fraction ranges up to 65%.

The two-conductivity probe is shown in Fig. 2. Two sensing element are made of teflon-coated stainless steel wires with a diameter of 0.076 mm and their tips are sharpened to a conical shape for minimizing the deformation of bubbles on impact with the probe. Each sensing wire is inserted into a 0.4 mm stainless steel tube, and fixed by a high temperature epoxy. Then the two sensors are inserted into a 1.6 mm stainless steel tube, and aligned in the axial direction of channel.

The proper distance between two sensor tips is critical for measuring the vapor bubble velocity with sufficient accuracy. It should be properly selected by considering the bubble motion and the sampling rate of A/D converter. If the distance is too small, inaccuracies in time duration measurements may be caused unless very high sampling frequency of A/D converter is supported. On the other hand, if the distance is too large, a vapor bubble cut by the front sensor may miss the rear sensor, or bubbles which do not pass the front sensor, may cut in. Most previous investigators have used a distance of 5 mm in their vertical adiabatic bubbly flow experiments. However, more attention should be paid to determine the distance in case of boiling flow because vapors can be generated on the heated surface in the space between two sensor tips. Preliminary experiments in boiling channel showed that the distance of 5 mm was too large for the present experiments since the difference in void fractions measured by front and rear sensors was found to be large near the heated surface, especially for local void fraction above $\sim$40%. In the present experiments, from the results of the preliminary test results obtained by using different distances in boiling channel and the additional high speed photography of an air bubble motion between two sensor tips in air–water flow, the appropriate distance was decided to be 1.5–2 mm. During the experiments, the distance and the sampling rate were set to be 1.6 mm and 25 kHz, respectively.

The change of resistivity sensed by each sensor was converted into voltage drop by an AC rectifier circuit. Generally, the voltage signals deviate from the ideal two-state square-wave signals mainly due to the finite size of the sensor and the possible deformation of the vapor bubble interface before the sensor enters from one phase to the other. Thus, the proper threshold voltage indicating the boundary between the two phases has to be used as a phase discrimination

criterion. In this study, the threshold voltage is calculated based on the pulse height and slope criterion for each bubble. The threshold voltage for each bubble is assumed to be proportional to the pulse height produced by an individual bubble, and is calculated as follows:

$$H_T = S(H_G - H_L) + H_L \tag{1}$$

In Eq. (1), H_T is the threshold voltage, S is the proportional constant, H_G and H_L and are the voltage levels by vapor and liquid phases, respectively. Even though a pulse is treated as a bubble by the threshold voltage, multipeaked signals above the threshold voltage can exist, which can be caused by multibubble contact or wetting of the probe tips. These bubbles are discriminated as separate bubbles by the slopes of the signals. Main advantage of the present algorithm is that the threshold voltage for each bubble is varied in accordance with the signal drift induced by probe fouling, change of flow condition and water conductivity.

The proportional constant was pre-determined by air–water experiments in the transparent tube with two quick closing valves. The local void fractions were measured by using the proportional constants of 0.1–0.9, and then area-averaged values were compared with the void fraction by the quick closing valve technique. From the comparison, the optimum proportional constant was determined to be 0.35. The local void fraction was determined by dividing the accumulated time that the probe sensor was exposed to the vapor phase by the total sampling time. The total sampling time should be sufficiently long enough for statistical treatment. The local void fraction was found to be nearly constant after about 20 s of integration time. In the present experiments, total sampling time for each local position was set to be 1 min, which is long enough to satisfy the repeatability of void fraction. Also, the uncertainty associated with local void fraction measurement was estimated to be $\pm 3\%$.

The local vapor velocity, more exactly bubble interface velocity, can be calculated by taking into account the time difference between the upstream and downstream signal, and the distance between the tips of two sensors. However, the two signals detected by the front and rear sensors do not always correspond to the same vapor, and the resident time intervals of vapor at both sensors are not the same. Thus, the signal validation is necessary for judging whether the signals from both sensors originate from the same vapor. In this study, if the ratio of vapor resident times at the front and the rear sensors was between 0.8 and 1.2 within the prescribed upper and lower limiting vapor resident times which were estimated by the combination of the probe distance and flow condition, then the two signals detected by both sensors were considered to have originated from the same vapor. For the estimation of error associated with the vapor bubble velocity measured by the two-conductivity probe, separate air–water experiments were conducted in a transparent tube where a porous stick ejecting air bubbles was inserted to simulate the boiling. The local velocity of a bubble ejected out of a hole on the porous stick was measured by the two-conductivity probe, and it was compared with that measured simultaneously by high-speed photography with the speed of 2000 frames/s. From the comparison, the error in velocity measurement was estimated to be $\pm 3.3\%$.

2.2.2. Pitot tube method

The local liquid velocity was measured by a Pitot tube. Although most applications have been limited to single-phase flow condition, some investigators applied this method to two-phase flow,

and suggested various models. In this study, the following model suggested by Bosio and Malnes (Reimann et al., 1983) was used for the measurement of local liquid velocity.

$$V_L = \frac{1}{\sqrt{(1-\varepsilon^2/2)}}\sqrt{\frac{2\Delta P}{K\rho_L}} \tag{2}$$

In Eq. (2), V_L is the liquid velocity, ΔP is the pressure difference between stagnation pressure and static pressure at the tube, ρ_L is the liquid density, ε is the local void fraction and K is the momentum transfer factor. Measurement of K is required for the local measurement in low velocity region because the drag force at Pitot tube tip can change rapidly with the liquid velocity. This factor was determined as a function of Reynolds number at Pitot tube in the pre-test of single-phase liquid flow.

The problems encountered when using Pitot tube in two-phase flow are the bubble inflow into the tube and the disturbance of flow field by the tube. For minimizing the possibilities of the problems, a 1/16″ Pitot tube (United Sensor) with a diaphragm exchangeable type differential pressure transducer (Validyne DP103 with CD15 demodulator) was used. Also, the cold-water injection unit was used to remove the air or vapor entrapped in the tube.

For testing the applicability of the liquid velocity calculation model, air–water experiments were conducted in the test channel. The local liquid velocities were measured using Eq. (2), and then the area-averaged values were compared with the average liquid velocities obtained by volume measurements. The comparison indicated that the mean error was ±1.75%.

3. Experimental results

Experiments were carried out at different values of mass flux (476–1061 kg/m^{2}s), heat flux (114.8–320.4 kW/m^2) and inlet subcooling (11.5–21.3 °C). Prior to the measurements, the dissolved gas was eliminated by the procedure of boiling and venting. After extensive degassing, the system was adjusted to the desired operating mass flux, inlet temperature and heat flux. The system pressure was maintained at 1–2 bar, and it was not controlled but determined by net volume expansion balanced by the bubble generation rate in the test channel and the ventilation rate in the storage tank. The measurements were performed at steady state condition, and a total of 21 sets of experiments was performed. Also, measuring positions was chosen as 13 points along the radial direction.

3.1. Radial distributions of local void fraction

The void fraction is one of fundamental parameters which characterize the structure of flow boiling because it reflects the energy of fluid and influences the distributions of other local parameters. The radial profiles of local void fraction are represented in Fig. 3. In the figure, $(r-R_i)/(R_0-R_i)=1$ indicates the inner surface of outer tube and $(r-R_i)/(R_0-R_i)=0$ means the heated surface. Also, the symbols, $\langle\varepsilon\rangle$, G, ΔT_{sub}, and q'' represent the area-averaged void fraction, mass flux, inlet subcooling and heat flux, respectively.

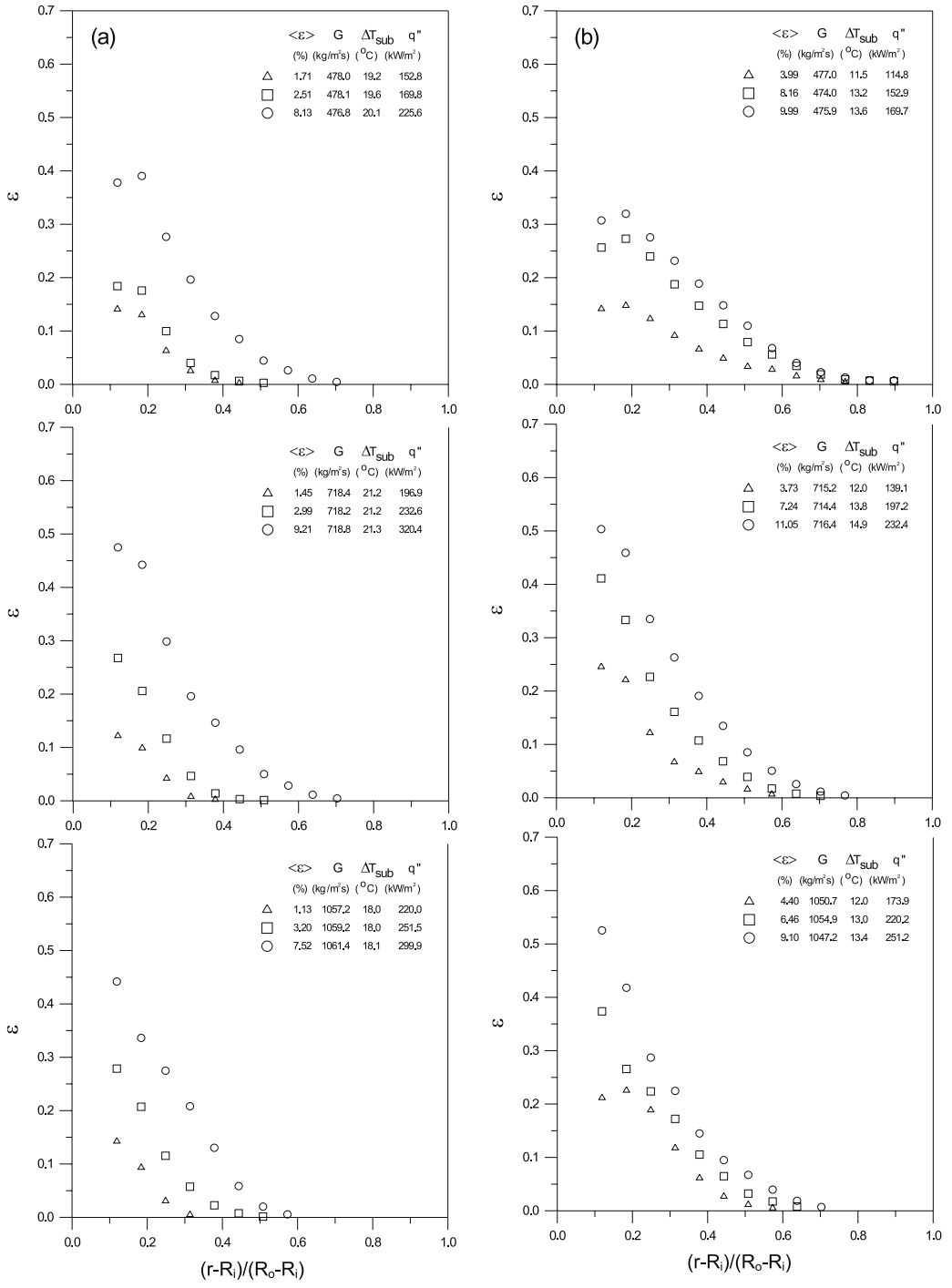

Fig. 3. Radial distributions of local void fraction: (a) high inlet subcooling; (b) low inlet subcooling.

One of the unique characteristics of the subcooled boiling is the existence of two distinguishable flow regions made by the thermal nonequilibrium of two phases. One is the bubble boundary layer as the two-phase region adjacent to a heated surface and the other is the subcooled liquid core. The thickness of bubble boundary layer is affected by inlet subcooling, mass flux and wall heat flux, and mainly dependent on the bubble size (Jiji and Clark, 1964) which can be determined by a balance of bubble coalescence and condensation rates.

The profiles in Fig. 3 show typical void fraction distributions in the subcooled boiling flow. The local void fraction decreases from the heated surface to the subcooled liquid core. The peak local void fraction is always observed near the heated surface. The peak value of the void fraction near the heated surface is quite different from the wall void peaking phenomena observed in the air–water bubbly flow, which is due to the migration of bubbles toward the wall. In subcooled boiling, high local void fraction near the heated surface is explicitly due to a large number of bubbles generated from the boiling sites on the heated surface. Many bubbles of small size are generated from the boiling sites of heated surface and then each bubble is detached from the surface when a bubble size exceeds a certain critical size. The detached bubbles will migrate laterally toward the subcooled liquid core under the competing process of bubble coalescence and condensation. The bubbles migrating to the subcooled liquid core will be condensed by the subcooled water, and thus the local void fraction decreases as moving toward the subcooled liquid core. Considering the boundary between bubble boundary layer and subcooled liquid core to be an intersection of abscissa and zero value of void fraction, the figure shows that the thickness of bubble boundary layer increases with the wall heat flux, and decreases with inlet subcooling and mass flux.

The effect of inlet subcooling on the void fraction profiles is described in Fig. 4. In the figure, the profiles for similar area-averaged void fraction and mass flux conditions are represented. The local void fraction near the heated surface in high inlet subcooling is larger than that in low inlet subcooling because larger heat flux is required for higher inlet subcooling to obtain same average void fraction, and thus more bubbles are expected to be generated. However, as moving to the subcooled liquid core, more bubbles are condensed in high inlet subcooling condition. Thus, the local void fraction in high inlet subcooling becomes smaller than that in low inlet subcooling as approaching the subcooled liquid core. The effect of mass flux is illustrated in Fig. 5 for similar area-averaged void fraction and inlet subcooling conditions. Its effect is the same as that of inlet subcooling; the higher local void fraction near the heated surface in high mass flux condition than that in low mass flux condition due to the larger heat flux required for higher mass flux condition to obtain same average void fraction. As mass flux increases, interfacial heat transfer can be enhanced. Thus, more bubbles are condensed in higher mass flux condition approaching the subcooled liquid core.

3.2. Radial distributions of local vapor and liquid velocities

The radial profiles of the axial components of local vapor velocity, V_G are shown in Fig. 6. There are no peaks corresponding to those observed near the heated surface in void fraction profiles. Also, the changes in the velocity profile are quite small compared with changes in the void fraction. The vapor bubble velocity increases moving toward the center of the channel gap and then decreases toward the outer wall. The bubbles in the bubble boundary layer with a higher average void fraction move faster than the bubbles in a lower average void fraction bubble layer

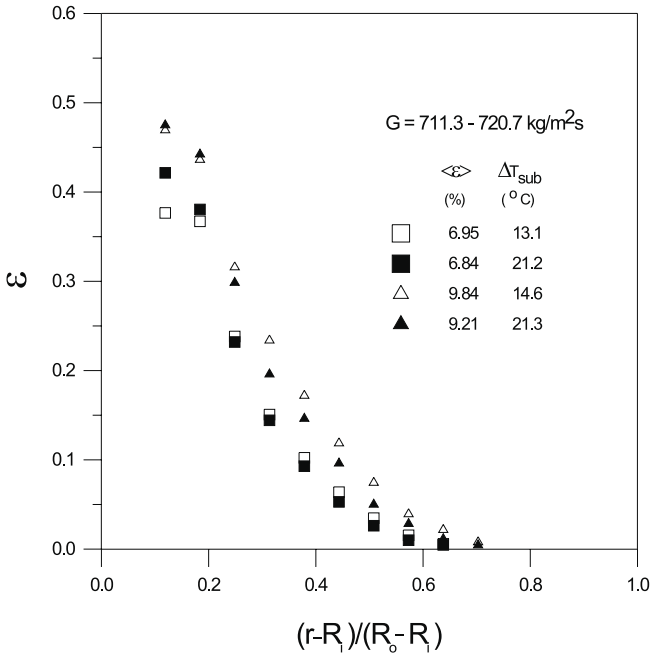

Fig. 4. Inlet subcooling effect on void fraction profiles.

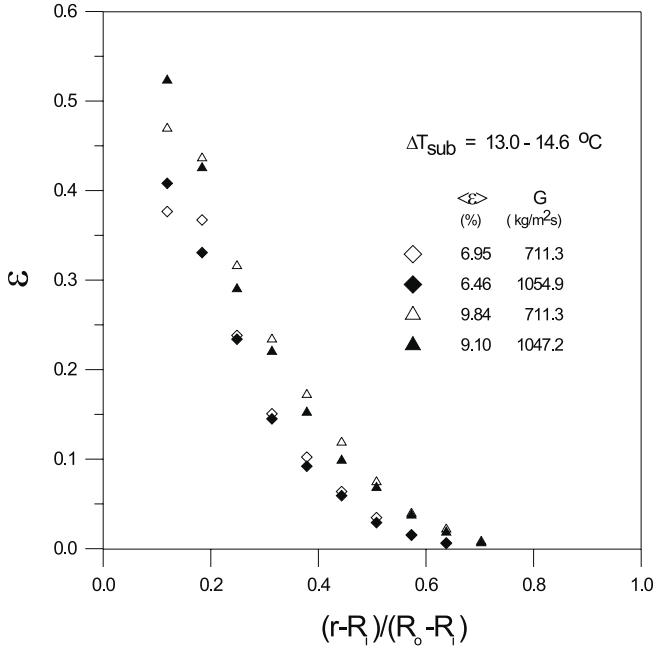

Fig. 5. Mass flux effect on void fraction profiles.

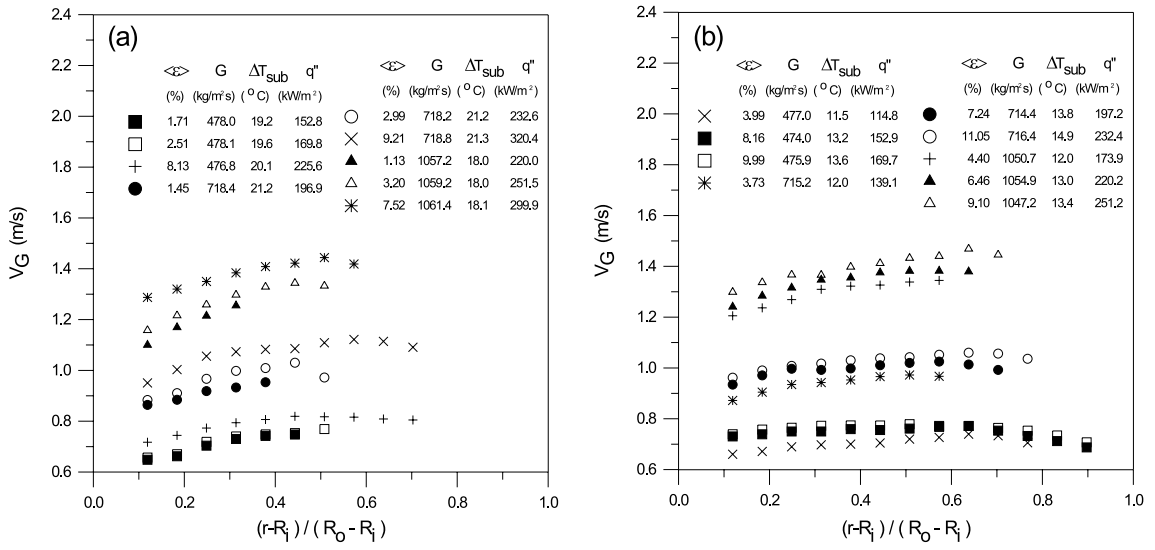

Fig. 6. Radial distributions of local vapor velocity: (a) high inlet subcooling; (b) low inlet subcooling.

for similar mass flux and inlet subcooling conditions. This can be expected since the average bubble size is larger at the higher void fraction bubble layer, and the buoyancy effect is enhanced for larger bubbles. Inlet subcooling effect can be seen in Fig. 6, for similar mass flux and heat flux conditions. The present data shows consistently that the vapor bubble velocity at lower inlet subcooling is larger than that at higher inlet subcooling. This is a reasonable trend since, for the same mass flux and heat flux, the average void fraction is larger at a lower inlet subcooling, and the average bubble size is larger.

In this study, to confirm the measured vapor velocity profiles, some bubbles in bubble layer were traced by high-speed photography. The experiments were conducted for mass flux of 470–718 kg/m^{2}s, inlet subcooling of 10–19 °C and heat flux of 88–170 kW/m^2. The photography was performed at a speed of 1024 frames/s using a high-speed video camera. The typical result is shown in Fig. 7. The average bubble sizes increase as approaching the center of the channel gap and a larger bubble of two bubbles indicated by two arrows moves faster than a smaller bubble. Thus, it was confirmed that the vapor velocity increases as moving from the heated surface to the center of the channel gap.

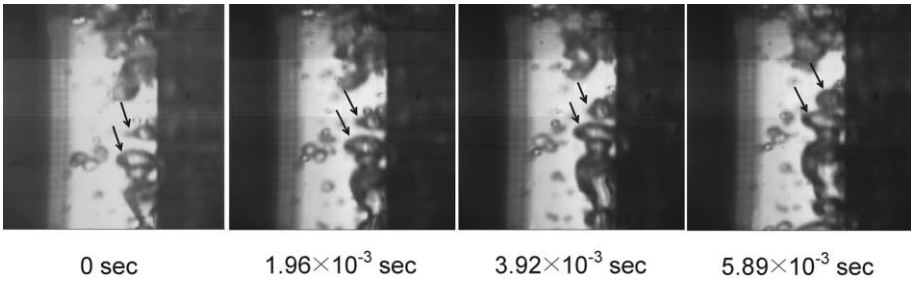

Fig. 7. Bubbles in bubble boundary layer: $G = 470$ kg/m^{2}s, $\Delta T_{sub} = 10$ °C, $q'' = 88$ kW/m^2.

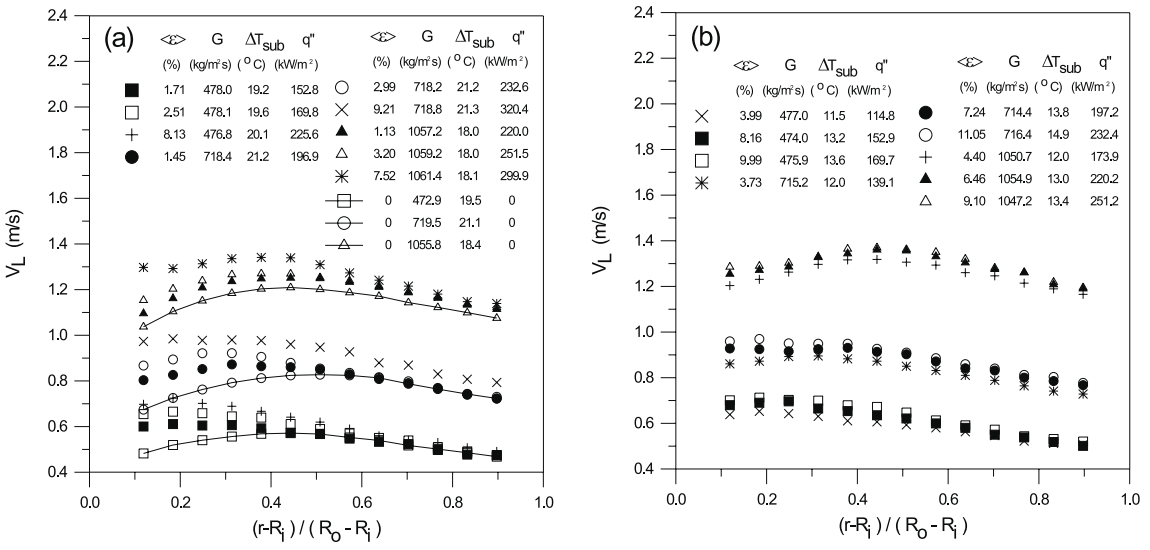

Fig. 8. Radial distributions of local liquid velocity: (a) high inlet subcooling; (b) low inlet subcooling.

The radial profiles of local liquid velocity, V_L, are shown in Fig. 8 where the profiles in single-phase flow with no heat addition are also represented. In case of single-phase flow, the liquid velocity has a maximum near the center of the channel gap and decreases toward both walls due to the effect of shear force at the channel wall. In boiling two-phase flow, the liquid velocity profile generally deviates from the velocity profile of single-phase flow due to the nonuniform void fraction and vapor velocity distributions. The location of maximum velocity moves toward the heated inner wall. However, as the mass flux increases, the profiles of liquid velocity gradually approach those of single-phase flow. Inlet subcooling effect can also be seen in the figure. The liquid velocity increases as the inlet subcooling decreases. This is a consistent result because, as shown in Fig. 6, the vapor bubble velocity increases as inlet subcooling decreases.

As a method for checking the applicability of Pitot tube method to the boiling experiments, the global continuity check was undertaken by comparing the inlet mass flow rate and the mass flow rate at the measuring plane. Since the contribution of vapor mass flow rate to total mass flow rate at the measuring plane is negligibly small compared with liquid mass flow rate (the maximum ratio of vapor to liquid mass flow rate is 0.016% in the present experiments), the mass balance calculation can be a method for confirming the applicability of Pitot tube method in the average sense. The inlet mass flow rate was measured by the turbine flowmeter, and the flow rate at the measuring plane was calculated by using the measured void fraction and velocities of both phases. The mean deviation between the values obtained from flow rate measurements and those calculated from the measured parameters was found to be $\pm 3.2\%$, and the difference was less than 5% in all cases.

4. Comparisons with calculations of a three-dimensional two-fluid model

Experimental results have been compared with the calculations of a three-dimensional two-fluid model of turbulent subcooled boiling flow. For this purpose, the general purpose CFD (Com-

putational Fluid Dynamics) code, CFX-4.2 (AEA Technology, 1997), was employed. In this code, body-fitted coordinates are included to allow the treatment of arbitrary complex geometries and the coordinate transformation is given numerically. The basis of the code is a conservative finite volume method with all variables defined at the center of control volumes which fill the physical domain being considered, and space discretization follows a structured mesh.

The two-fluid model in CFX-4.2 is formulated in terms of two sets of governing conservation equations. These are the averaged balance equations for mass, momentum and energy in each phase. The governing equations are complemented by various closure relations for the interfacial transfer rates of mass, momentum and energy as well as turbulence terms in the field equations. The subcooled boiling model in the code assumes incompressible flow at a constant absolute pressure. The saturation temperature and the latent heat of evaporation are specified at this pressure. The model uses constant physical properties evaluated at the saturation temperature. The bubble diameter, d, required to estimate the interfacial transfer terms is assumed to vary linearly with local liquid subcooling as follows (Anglart and Nylund, 1996):

$$d = \frac{d_1 - d_0}{T_1 - T_0} T_{\text{sub}} + \frac{d_0 T_1 - d_1 T_0}{T_1 - T_0} \tag{3}$$

In Eq. (3), T_{sub} is the local liquid subcooling, and d_0 and d_1 are the bubble diameters at reference liquid subcoolings, T_0 and T_1, respectively. The details of governing equations and closure relations can be found in the code manual.

For the calculations, the radial direction of flow domain was divided into 14 uniform meshes, the axial direction into 30 uniform meshes and the azimuthal direction into four uniform meshes. The liquid phase was represented as continuous phase and the vapor as dispersed phase. The continuous liquid phase was modeled as turbulent and the dispersed vapor phase was assumed to be laminar. At the inlet boundary, the velocity profiles of both phases were assumed to be flat, and given by the measured average liquid velocity. The temperature of liquid was given by the measured inlet liquid temperature. At the outlet which is the end of heated section, the pressure boundary condition was set using the measured absolute pressure. The dynamic boundary condition at the wall was given as for single-phase flow. A laminar and a turbulent sublayer were assumed to be present for liquid phase. Also, no slip condition at the wall was applied. The thermal boundary condition at the heated wall was given as the measured heat flux. The outer wall of annulus was assumed to be adiabatic.

The calculations were performed in order to assess the capability of the implemented two-phase models. Because the interfacial transfer terms are extremely important for predicting two-phase flow field, various models related with interfacial momentum transfer, interfacial heat transfer and bubble size which is essential to the interfacial transfer terms were tested using the models included in the code. The evaluation indicated that most of the tested models were not very sensitive to the calculation results, but the bubble size was found to have a significant effect on the predictions. The typical results of bubble size effect are represented for the profile of void fraction in Fig. 9. In these calculations, the drag force between the vapor bubbles and the continuous fluid was considered according to the model proposed by Ishii and Zuber (1979). Also, nondrag force such as lift force, turbulent dispersion force and wall lubrication force were included. Heat transfer across a phase boundary was modeled in terms of the interfacial heat transfer coefficient by Lanz and Marshall (1952). The reference liquid subcoolings (T_0 and T_1) in Eq. (3) were taken as

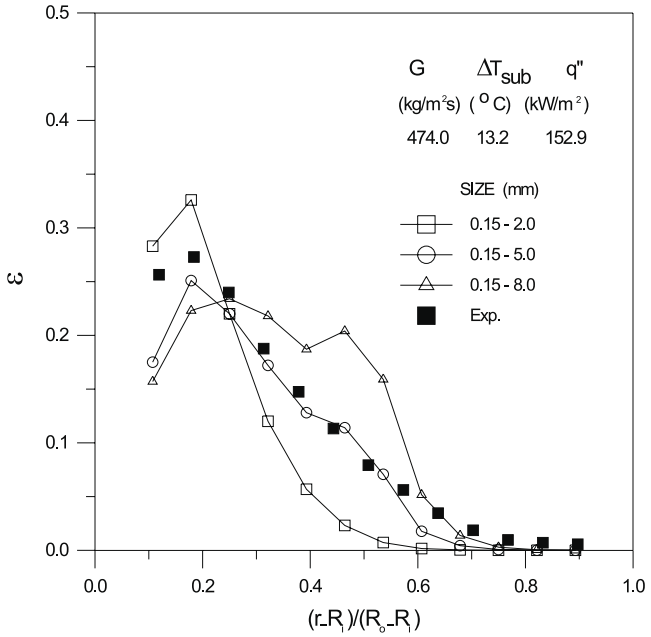

Fig. 9. Effect of bubble size on void fraction profiles.

13.5 and −5 K, respectively, as recommended in CFX-4.2. As shown in the figure, the small upper limit (2.0 mm) for bubble size under-predicted the measured values away from the inner heated wall, and the large upper limit (8.0 mm) has resulted in unrealistic void fraction trend. 5 mm of upper limit gave reasonable prediction compared with other two cases. This fact indicates that predictions are highly influenced by the selection of appropriate user-defined bubble diameters. Thus, bubble size model by Eq. (3) will certainly place limitations on the general application of the subcooled boiling model. The distributions of predicted bubble diameters corresponding to Fig. 9 are illustrated in Fig. 10. The calculated bubble size is nearly constant or slightly increases as approaching the heated surface due to the decrease of liquid subcooling. However, as reported in subcooled boiling of R-113 by Roy et al. (1994), the vapor bubbles which are relatively small near the heated surface increases due to the bubble coalescence as they move away from the surface and then decreases toward outer adiabatic wall due to the condensation. Thus, although it can be expected that the bubble size model taking into account only liquid subcooling can be applied for relatively low heat flux condition, the bubble size model considering the bubble coalescence/condensation should be accommodated to estimate accurate interfacial transfer terms for general application.

More comparisons are represented in Figs. 11–13 for void fraction, vapor velocity and liquid velocity, respectively. In those calculations, the upper limit for bubble diameter was taken to be 5 mm. As shown in Fig. 11, the calculation results obtained for void fraction are reasonable in a wide range of conditions: heat flux, mass flux and inlet subcooling level. However, except for liquid velocity in low flow conditions, the calculations for the velocities could not predict the measurements well. This underlines the need for improvements of dynamic models for momentum

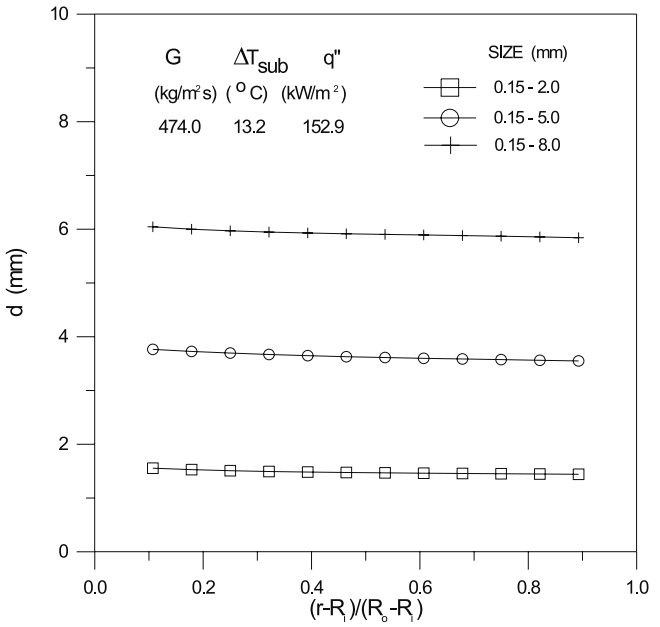

Fig. 10. Predicted bubble diameter distributions.

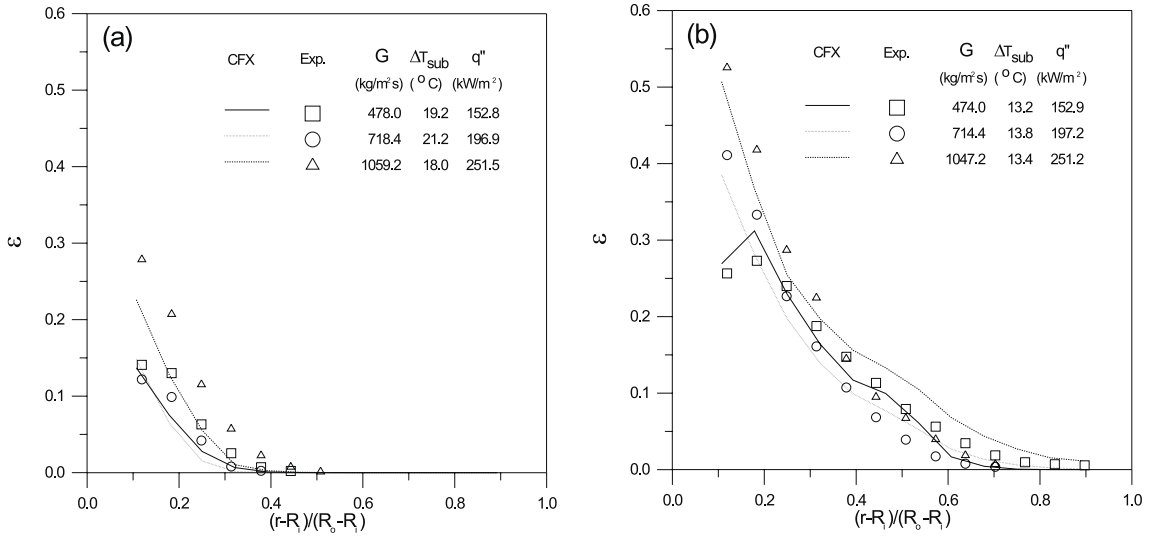

Fig. 11. Comparison of calculation results with measurements for void fraction: (a) high inlet subcooling; (b) low inlet subcooling.

transfer. Also, as stated previously, it is necessary that a bubble size model should be developed, which takes into account bubble coalescence.

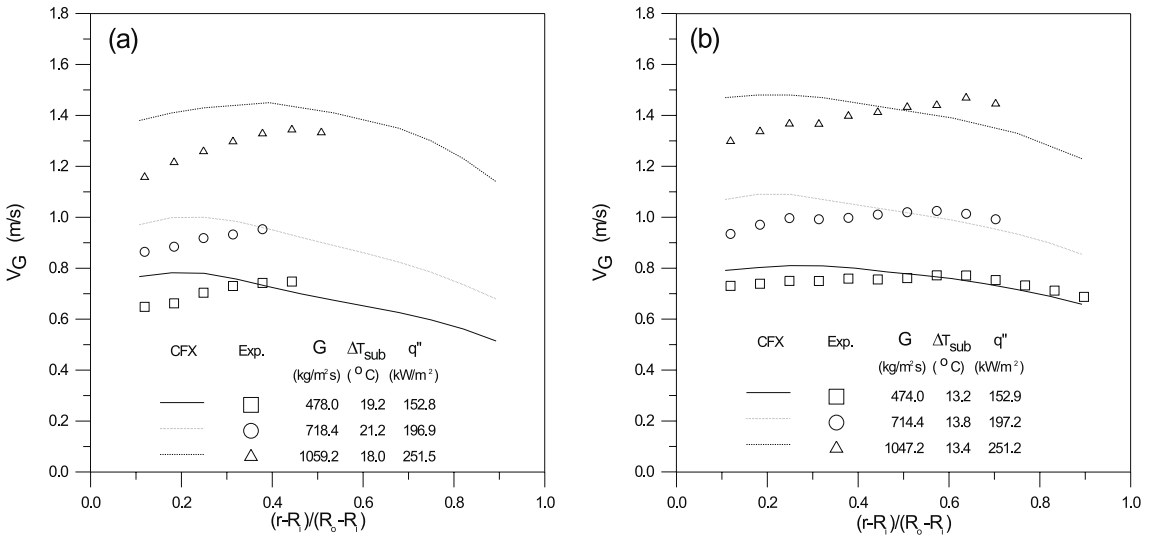

Fig. 12. Comparison of calculation results with measurements for vapor velocity: (a) high inlet subcooling; (b) low inlet subcooling.

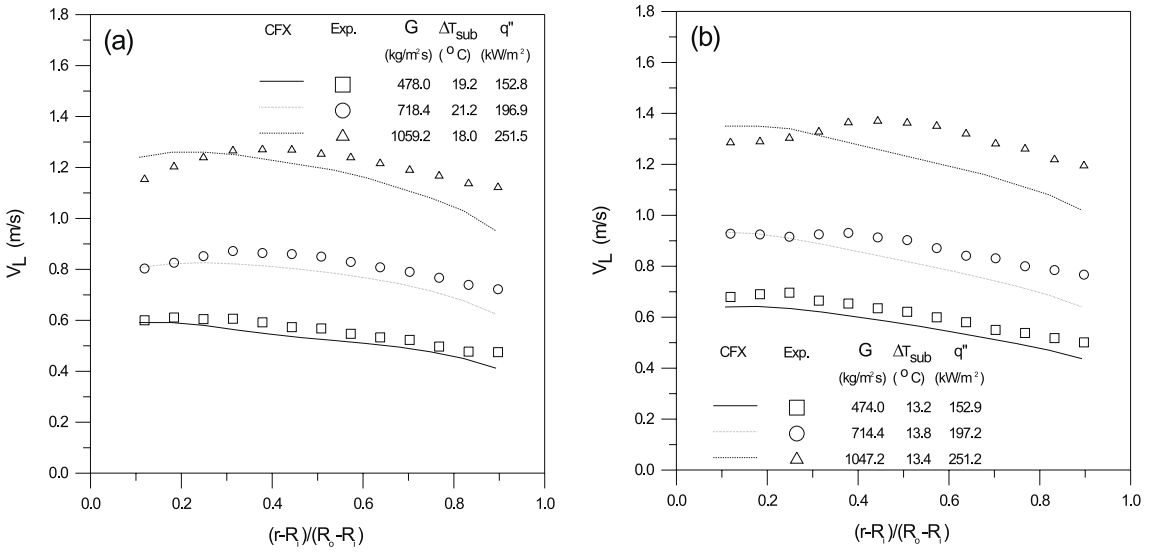

Fig. 13. Comparison of calculation results with measurements for liquid velocity: (a) high inlet subcooling; (b) low inlet subcooling.

5. Conclusions

The radial characteristics of local void fraction, vapor velocity and liquid velocity were experimentally investigated in vertical concentric annulus for the subcooled boiling flow of water.

Also, some results were compared with the predictions by multidimensional two-fluid model of subcooled boiling in CFX-4.2.

Measurements showed that the local void fraction decreased from the heated surface to the subcooled liquid core. Also, the bubble boundary layer increased with heat flux, and decreased with inlet subcooling and mass flux. As the inlet subcooling or mass flux increased, the peak void fraction near the heated surface increased. However, as moving toward subcooled liquid core, the local void fraction in high inlet subcooling or high mass flux condition became smaller than that in low inlet subcooling or low mass flux condition. The vapor velocity increased moving toward the center of the channel gap, and then decreased toward the outer wall. The vapor velocity at lower inlet subcooling was larger than that at higher inlet subcooling. The liquid velocity profiles generally deviated from the profiles of single-phase flow due to the nonuniform void fraction and vapor velocity distributions. However, as the mass flux increased, the profile of liquid velocity gradually approached that of single-phase flow.

Numerical simulation of subcooled flow boiling using CFX-4.2 yielded reasonable results on void fraction if appropriate bubble diameters were selected but some discrepancies in vapor and liquid velocities. Further modeling work is required for estimating the accurate interfacial transfer terms.

Acknowledgements

This work was performed under auspices of Nuclear R&D program by the Korean Ministry of Science and Technology.

References

AEA Technology, 1997. CFX-4.2 Solver manual.

Anglart, H., Nylund, O., 1996. CFD application to prediction of void distribution in two-phase bubbly flows in rod bundles. Nucl. Eng. Des. 163, 81–98.

Briere, E., Larrauri, D., Olive, J., 1995. ASTRID: A 3D eulerian software for subcooled boiling flow modeling—Comparison with experimental results in tubes and annuli. In: Proc. NURETH-7, vol. 1. Saratoga, NY, pp. 736–749.

Delhaye, J.M., Semeria, R., Flamand, J.C., 1973. Void fraction and vapor and liquid temperatures; Local measurements in two-phase flow using a microthermocouple. ASME J. Heat Transfer 95, 365–370.

Hasan, A., Roy, R.P., Kalra, S.P., 1991. Some measurements in subcooled flow boiling of Refrigerant-113. ASME J. Heat Transfer 113, 216–223.

Herringe, R.A., Davis, M.R., 1976. Structural development of gas–liquid mixture flows. J. Fluid Mech. 73, 97–123.

Hino, R., Ueda, T., 1985. Studies on heat transfer and flow characteristics in subcooled flow boiling—Part2. Flow characteristics. Int. J. Multiphase Flow 11, 283–297.

Ishii, M., Zuber, N., 1979. Drag coefficient and relative velocity in bubbly, droplet or particulate flows. AIChE J. 25, 843–855.

Jiji, L.M., Clark, J.A., 1964. Bubble boundary layer and temperature profiles for forced convection boiling in channel flow. ASME J. Heat Transfer 86, 50–58.

Kataoka, I., Ishii, M., Serizawa, A., 1986. Local formulation and measurements of interfacial area concentration in two-phase flow. Int. J. Multiphase Flow 12, 505–529.

Kocamustafaogullari, G., Wang, Z., 1991. An experimental study on local interfacial parameters in a horizontal bubbly two-phase flow. Int. J. Multiphase Flow 17, 553–572.

Lanz, W.E., Marshall, W.R., 1952. Evaporation from drop. Chem. Eng. Prog. 48, 173–180.

Liu, T.J., 1989. Experimental investigation of turbulence structure in two-phase bubbly flow. Ph.D. Thesis, Northwestern University, Evanston, Ill.

Neal, L.G., Bankoff, S.G., 1963. A high resolution resistivity probe for determination of local void properties in gas–liquid flow. AIChE J. 9, 490–494.

Reimann, J., Kusterer, H., Jhon, H., 1983. Two-phase mass flow rate measurements with Pitot tube and density measurements. Symp. Measuring Techniques in Gas–Liquid Two-Phase Flows, Nancy, France.

Revankar, S.T., Ishii, M., 1992. Local interfacial area measurement in bubbly flow. Int. J. Heat Mass Transfer 35, 913–925.

Roy, R.P., Velidandla, V., Kalra, S.P., 1997. Velocity field in turbulent subcooled boiling flow. ASME J. Heat Transfer 119, 754–766.

Roy, R.P., Velidandla, V., Kalra, S.P., Peturaud, P., 1994. Local measurements in the two-phase region of turbulent subcooled boiling flow. ASME J. Heat Transfer 116, 660–669.

Sekoguchi, K., Tanaka, O., Esaki, S., Katsuki, N., Nakasatomi, M., 1981. Prediction method of flow patterns in subcooled and low quality boiling regions. Bull. JSME 24 (191), 834–841.

Serizawa, A., Kataoka, I., Michiyoshi, I., 1975. Turbulence structure of air–water bubbly flow—I. Measuring techniques. Int. J. Multiphase Flow 2, 221–233.

Velidandla, V., Putta, S., Roy, R.P., 1996. Velocity field in isothermal turbulent bubbly gas–liquid flow through a pipe. Exp. Fluids 21, 347–356.

Welle, R.V., 1985. Void fraction, bubble velocity and bubble size in two-phase flow. Int. J. Multiphase Flow 11, 317–345.